3-31-2022

Ultra-broadband and polarization-insensitive metasurface absorber with behavior prediction using machine learning

Shobhit K. Patel

Juveriya Parmar

Vijay Katkar

Fahad Ahmed Al-Zahrani

Kawsar Ahmed

Alexandria Engineering Journal (2022) 61, 10379–10393

HOSTED BY

Alexandria University

Alexandria Engineering Journal

www.elsevier.com/locate/aej
www.sciencedirect.com

Ultra-broadband and polarization-insensitive metasurface absorber with behavior prediction using machine learning

Shobhit K. Patel [a], Juveriya Parmar [a,b], Vijay Katkar [a], Fahad Ahmed Al-Zahrani [c], Kawsar Ahmed [d,e,*]

[a] *Department of Computer Engineering, Marwadi University, Rajkot, Gujarat, India*
[b] *Department of Mechanical and Materials Engineering, University of Nebraska-Lincoln, NE 68588, USA*
[c] *Computer Engineering Department, Umm Al-Qura University, Mecca 24381, Saudi Arabia*
[d] *Group of Bio-photomatiχ, Department of Information and Communication Technology, Mawlana Bhashani Science and Technology University, Santosh, Tangail-1902, Bangladesh*
[e] *Department of Electrical and Computer Engineering, University of Saskatchewan, 57 Campus Drive, Saskatoon, SK S7N 5A9, Canada*

Received 18 December 2021; revised 8 February 2022; accepted 31 March 2022

KEYWORDS

Absorber;
Metasurface;
GST;
Ultraviolet;
Visible;
Infrared;
Machine learning

Abstract The solar spectrum energy absorption is very important for designing any solar absorber. The need for absorbing visible, infrared, and ultraviolet regions is increasing as most of the absorbers absorb visible regions. We propose a metasurface solar absorber based on $Ge_2Sb_2Te_5$ (GST) substrate which increases the absorption in visible, infrared and ultraviolet regions. GST is a phase-changing material having two different phases amorphous (aGST) and crystalline (cGST). The absorber is also analyzed using machine learning algorithm to predict the absorption values for different wavelengths. The solar absorber is showing an ultra-broadband response covering a 0.2–1.5 μm wavelength. The absorption analysis for ultra-violet, visible, and near-infrared regions for aGST and cGST is presented. The absorption of aGST design is better compared to cGST design. Furthermore, the design is showing polarization insensitiveness. Experiments are performed to check the K-Nearest Neighbors (KNN)-Regressor model's prediction efficiency for predicting missing/intermediate wavelengths values of absorption. Different values of K and test scenarios; C-30, C-50 are used to evaluate regressor models using adjusted R^2 Score as an evaluation metric. It is detected from the experimental results that, high prediction proficiency (more than 0.9 adjusted R^2 score) can be accomplished using a lower value of K in KNN-Regressor model. The design

* Corresponding author at: Department of Information and Communication Technology, Mawlana Bhashani Science and Technology University, Santosh, Tangail 1902, Bangladesh.
E-mail addresses: shobhitkumar.patel@marwadieducation.edu.in (S.K. Patel), juveriyaparmar2@gmail.com (J. Parmar), vijay.katkar@marwadieducation.edu.in (V. Katkar), fayzahrani@uqu.edu.sa (F.A. Al-Zahrani), kawsar.ict@mbstu.ac.bd (K. Ahmed).

Peer review under responsibility of Faculty of Engineering, Alexandria University.

https://doi.org/10.1016/j.aej.2022.03.080

results are optimized for geometrical parameters like substrate thickness, metasurface thickness, and ground plane thickness. The proposed metasurface solar absorber is absorbing ultraviolet, visible, and near-infrared regions which will be used in solar thermal energy applications.

1. Introduction

The increasing population has led to increased power demand which has increased the usage of fossil fuels that led to the global warming issues. So, to fulfill this increased energy demand renewable energy sources, particularly solar energy is required [1]. As solar energy is the cleanest and easily available renewable source, it is the dominant candidate to handle this issue [2]. Most of the available solar absorber designs gave absorption only for the visible region. So, the highly efficient and broadband solar absorber is desirable which not only covers visible region but also covers infrared region and ultraviolet region [3,4]. The two materials which can improve the absorption of solar absorber and needs to be investigated are metamaterial and phase change material. The broadband absorption required for solar absorber can be achieved by using metamaterials which is artificial material with some unusual properties and the second material (Phase change material) can be used to increase the absorption and tune the absorption response. A literature discussion on these metamaterials and phase change material related to solar absorbers is added for clarity here.

Metamaterials with their unique electrical and optical properties have gained interest amongst many researchers. Metamaterials are playing a vital role nowadays in designing many microwave and optical absorbers. Split ring resonators, thin wires are used as metamaterial components to improve the performance of many photonic components. Circular split rings as metamaterial elements can be used to absorb the microwave spectrum [5]. Metamaterials can be used in the metal–insulator-metal (MIM) structures to improve their absorption efficiency [6]. The metamaterials in four different nanotube forms are used to improve efficiency. The nanotube form of metamaterial improves the overall absorption of the structure [7]. The perfect absorber is investigated using graphene split-ring resonators as the resonating element. The absorption response using these graphene split-ring resonators clearly shows three absorption peaks with 99% of absorption or more in all three absorption peaks [8]. The tungsten nanowire-based metamaterial absorber is used for absorbing solar thermal energy [9]. Metasurfaces are 2D artificial surfaces that have the same abilities as their 3D counterparts with better perfect absorbing and other properties. Metasurfaces are used in many applications like sensing, imaging, energy harvesting, etc. [10–15]. Metasurface array can be used to improve absorption. Broadband absorption is achieved by incorporating metasurface with graphene material [16–19]. Ultra-broadband absorbers are needed to absorb a wide range of the spectrum. An Ultra-broadband absorber using an array of silicon metasurfaces is presented [20]. Titanium nitride metasurface can be used for designing solar absorbers. These metasurfaces show ultra-broadband response which covered the ultraviolet, visible, and near-infrared frequency region [21]. The ultra-broadband absorber is designed for ultraviolet to the near-infrared frequency spectrum. The design structure is achieving such high absorption by using connecting cylindrical holes [22]. Absorber using subwavelength resonators is designed for ultra-broadband absorption in the infrared region. The design gives 90% absorption for the selected infrared range [23]. Ultra-broadband microwave absorber is designed by placing metal trips in array form over a dielectric substrate. The absorber is designed to operate over the microwave frequency region [24]. Metamaterial perfect absorber designs with the ultra-broadband response and polarization sensitivity [13,14,25,26]. An aluminum slit array is placed over silicon dioxide and titanium period stacking to achieve ultra-broadband response [17]. Patel and co-authors reviewed graphene based absorbers for sensing, solar energy harvesting applications [27]. Patel et al. presented,metasurface based solar absorber with highest average absorption of 89%. Several other researchers also presented ultrabroadband highly efficient solar absorbers for solar energy harvesting, energy conversion applications [28–30].

Phase change materials are very important as the change in phase of the materials changes several properties of the design [31]. The change of phase can be used to change the polarization, absorption, etc. [32]. The phase change materials are used in many applications of photonics and plasmonics. The performance of absorbers can be enhanced using GST material. Tunable spectrum can also be achieved using phase change material. [33–35]. Phase change materials can be used to reconfigure optical metasurfaces by changing their phase. The resonances of plasmonics designs are shifted using phase change materials [36]. GST metasurfaces are used to tune the absorption spectrum and it also has polarization-independent behavior. The change in polarization does not change the absorption behavior of this GST metasurface[37].

The requirement of ultrabroadband solar absorber is very high because its coverage of most of the wavelength regions. Furthermore, due to high meshing conditions sometimes the simulation process takes longer time and to reduce this processing time and resources we have implemented machine learning based model to predict the intermediate wavelength values. We propose an ultra-broadband absorber that covers infrared, visible, and ultraviolet regions. The absorption analysis is presented for aGST and cGST. The average absorption is more than 92% for aGST phase. The absorption results are predicted using machine learning algorithms. The design is analyzed for absorption, reflection, phase change ratio, phase difference, impedance, and electric field. The design results for different polarization and the incident angle are also observed. Section 2 provides the design and results of the metasurface absorber. The machine learning prediction results are discussed and in Section 3. The conclusion is presented in Section 4.

2. Design and results

2.1. Metasurface absorber design

The metasurface-based solar absorber design based on phase change material is presented in this section. The detailed design schematic is presented in Fig. 1. The use of metasurface increases the absorption of solar absorbers. We have taken a square and circle as metasurface elements and created an array by placing them alternatively. The 3D and front views are shown in Fig. 1(a–b). The metasurface elements are placed above phase change material. We have used GST as phase-changing material and its amorphous and crystalline phases are observed in this manuscript. The metasurface elements are placed above GST material. The GST materials are based on a gold ground plane. The thickness of metasurface (M), substrate (S), and ground plane (G) is 0.4 μm, 0.6 μm and the ground plane is 0.2 μm. The surface observed is having the same length and width. The dimensions are $4 \times 4\ \mu m^2$.

2.2. Results and discussions

The results presented in this manuscript are analyzed using COMSOL multiphysics simulator based on the finite element method. The simulations conditions are: tetrahedral Delaunay tessellation condition with a maximum and minimum size of meshing is set as 150 nm and 15 nm respectively. The growth value of meshing is set as 0.6. The results of absorption, electric field, and phase change ratio (PCR), etc. are presented in Figs. 2–9. Periodic boundary conditions are applied to maintain the periodicity of the structure. The light falls on the structure from the top and most of the light is absorbed in the absorbing layer. The absorption response of the structure is presented in Fig. 2. The broadband absorption is achieved because of the combination of gold-GST structure which is used in the research. The resonator and substrate material gives the rise to absorption according to their structural design. The analysis of absorption for three solar spectrum regions is showing more than 90% absorption. The comparison of the absorption for ultraviolet, visible, and near-infrared regions is presented for both aGST and cGST in Table 1. The absorption results clearly show that aGST performs better over cGST. The average absorption for all three regions is above 90%. The highest absorption for the ultraviolet region and lowest for the near-infrared region. The total absorption is 92% for all three regions for aGST phase.

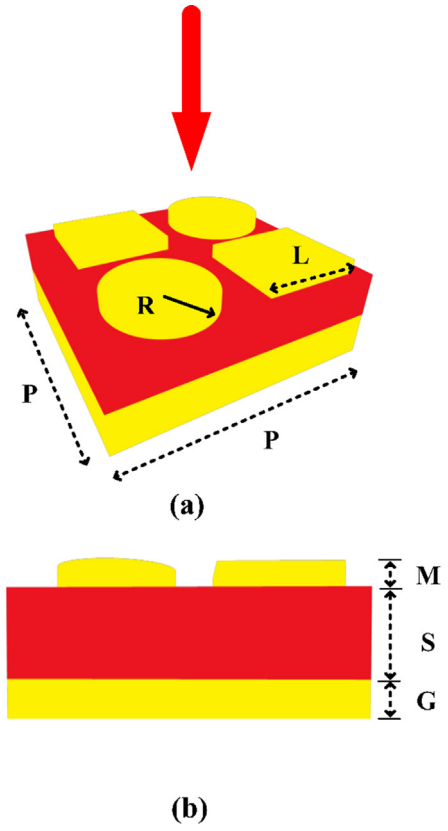

Fig. 1 Metasurface solar absorber design (a) 3D view of the design (b) 2D front view of the design. The array of alternate square and circle elements are used as metasurface. The metasurface is placed above GST phase change material supported by the ground plane. The different sizes of the structure are P = 4 μm, R = 0.7 μm, L = 1.4 μm, M = 0.4c, S = 0.6 μm, G = 0.2 μm.

The three metasurface designs square-circle metasurface, circle metasurface, and square metasurface designs are analyzed for the broad wavelength range. The results clearly show that the square-circle metasurface design shows better results compared to all other designs. The results are also compared in Table 2. The comparison shows that square-circle metasurface has the best absorption of 95.9%, 93.6%, and 90.6% for ultraviolet, visible, and near-infrared regions respectively. The main reason behind the high absorption rate of square-circle design is the combination of square and circle change in inductance and capacitance which will change the resonance which effects in high absorption.

The absorption of the metasurface absorber is analyzed for three geometrical parameters substrate thickness, metasurface thickness, and ground plane thickness, and presented in Figs. 4–6 respectively. We selected these three parameters because the variation in these three parameters changes the absorption results. Metasurface thickness changes overall resonance which affects the abruption of the structure. The substrate thickness improvement improves the absorption to a certain limit. The ground plane blocks the wave and transmission is minimum because of the thickness variation of the ground plane. The substrate thickness is varied from 0.2 μm to 1 μm to observe its effect on absorption. The absorption for color plot and line plot is shown in Fig. 4. The highest absorption is achieved for the 0.6 μm substrate thickness. The increase in thickness improves the absorption as presented in the result but after one point the improvement in thickness increases the inductance and it decreases the absorption. This is visible from the results presented in Fig. 4.

The metasurface thickness variation and its effect are shown in Fig. 5. The color plot and line plot are presented in Fig. 5(a) and (b) respectively. The metasurface thickness is varied from 0.1 μm to 0.6 μm. The response is presented for the 0.1 μm to 2.5 μm wavelength range. The result shows that the highest absorption is achieved for 0.4 μm substrate layer thickness. The lower thickness value gives low absorption results as presented in the response. The absorption above the 0.4 μm reduces the absorption as it changes the resonance of the metasurface structure.

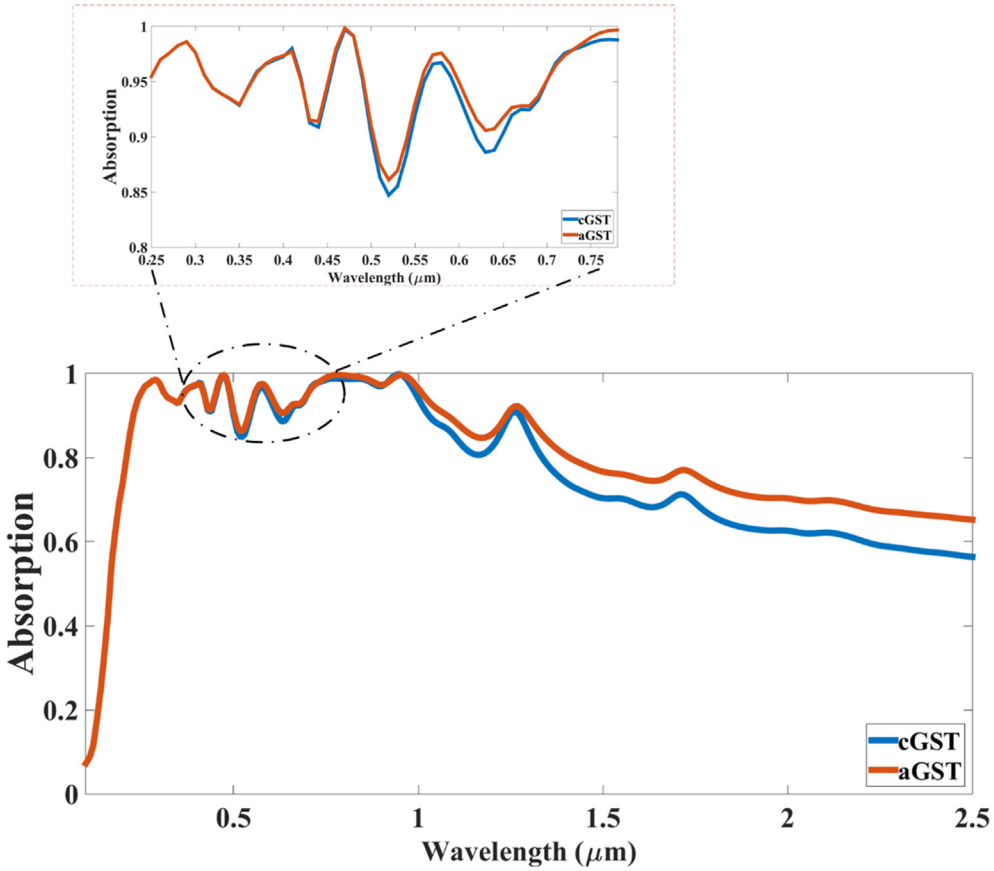

Fig. 2 Absorption response of metasurface solar absorber design for cGST and aGST phases. The wavelength range observed is 0.1–2.5 μm. Inset shows the absorption response for ultraviolet and visible region ranging from 0.25 μm to 0.78 μm. Absorption is more than 90% for visible and ultraviolet ranges.

The ground layer thickness variation and its effect on absorption are presented in Fig. 6. The color plot and line plot are presented in Fig. 6(a) and (b) respectively. The ground layer thickness is varied from 0.2 μm to 0.5 μm. The response is presented for the 0.1 μm to 2.5 μm wavelength range. The results clearly show that absorption variation is similar for different ranges of ground plane thickness. The ground plane does not let waves go through the ground plane and it reduces the transmission. The transmission is almost zero because of this ground plane.

We have also analyzed the electric field response in the substrate layer for different wavelengths and presented it in Fig. 7. The results are presented for four wavelengths (0.1 μm, 0.5 μm, 1 μm, and 1.5 μm). Results clearly show that for an initial wavelength of 0.1 μm the electric field is minimum as the substrate layer is not absorbing any light which is also visible through the absorption line plot. As the wavelength increases the electric field in the substrate layer is also increasing and it is visible through the 0.5 μm, 1 μm, and 1.5 μm electric field intensity response. The electric field intensity results are presented for 0.1 μm, 0.5 μm, 1 μm, and 1.5 μm. And if we observe the absorption response it is clear that at 0.1 μm, we achieve very low absorption, for 0.5 μm,1 μm and 1.5 μm, we achieve comparatively high absorption response which is validated by red color spreading all over the substrate surface in the electric field intensity from Fig. 7.

The calculation of polarization is given in Eqs. (1)–(4) [38,39]. The polarization conversion rate and phase change difference are the two parameters which can be used to check the polarization sensitiveness. The results of polarization conversion rate, phase change difference and reflectance results for polarized waves are presented in Fig. 8.

$$T_{ij} = \left| \frac{E_j^{Trans}}{E_i^{Inc}} \right| \quad (i,j = x,y) \tag{1}$$

$$R_{ij} = \left| \frac{E_j^{Reflec}}{E_i^{Inc}} \right| \quad (i,j = x,y) \tag{2}$$

$$\text{Polarization Conversion Rate (PCR)} = \frac{|R_{xy}|^2}{|R_{xy}|^2 + |R_{xx}|^2} \tag{3}$$

$$\Delta\Phi = \Phi_{xy} - \Phi_{xx} \tag{4}$$

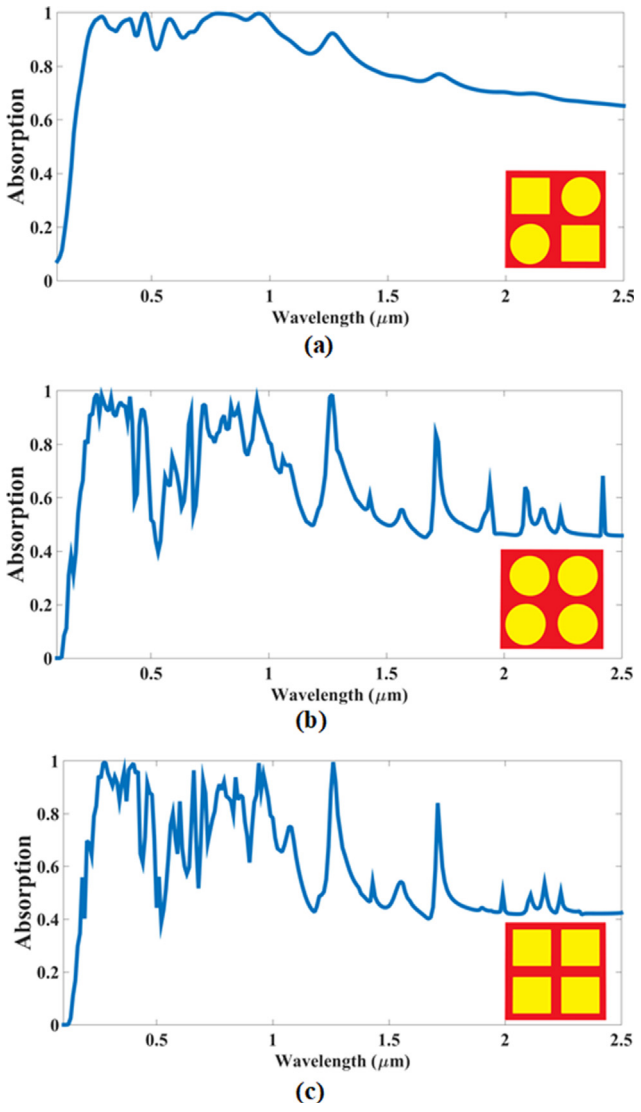

Fig. 3 Comparison of absorption (aGST) for three metasurface designs (a) Square-circle metasurface (b) Circle metasurface. Absorption is better for square-circle metasurface absorber design.

E_j^{Trans} (j = x, y) = Transmitted electric field
E_j^{Reflec} (j = x, y) = Reflected electric field
E_i^{Inc} (i = x, y) = Polarized incident wave electric field

R_{xx} and R_{xy} are co-polarized wave and cross-polarized wave used in Eqs. (1)–(4). The phase change for these co-polarized wave and cross polarized wave is presented in Eq. (4). The co-polarized and cross-polarized reflectance is presented in Fig. 8(a) and the polarization conversion rate (PCR) and phase change difference is presented in Fig. 8(b). The results clearly show that the structure is polarization-insensitive due to symmetrical structure of the proposed design.

The comparison of proposed absorber is shown in Table 3. The comparison is provided for absorption wavelength range, average absorption, polarization insensitiveness, and angular stability. The comparison clearly shows that our proposed design has better absorption compared to all other designs.

3. Machine learning prediction results

Machine learning is applied to predict the absorption values for different wavelengths. Python (version 3.8) and scikit-learn library (version 0.24) are used to perform the experiments [40]. The data obtained by the simulation process using COMSOL Multiphysics is used for experimentation and all regression models are trained using first-degree polynomial features.

Experiments are carried out to see if it is possible to anticipate absorption levels for various wavelengths under a variety of situations or not. Simulation resource requirements can be reduced if simulation is used to obtain absorption values for various wavelengths in a variety of conditions with a larger wavelength step size, and then machine learning-based regression models are used to predict values of absorption for in-between wavelengths.

Test scenarios, C-30 and C-50 are considered to evaluate the prediction efficiency of the KNN-Regressor module. In test scenario C-30, data generated during simulation is divided into two non-overlapping subsets. One subset contains randomly selected 30% simulation records whereas other contains 70% simulation records. Subset containing 70% simulation records is used to train KNN-Regressor model and other subset containing 30 simulation records are used to evaluate prediction proficiency of model. In test scenario C-50, data generated during simulation is divided into two equal-size non-overlapping subsets of simulation records. One subset contains even number rows and another contains odd number rows from available data. Anyone partition can be used to train KNN-Regressor model and other for testing the prediction efficiency of model.

Machine learning models are utilized in Test Scenarios C-30 and C-50 to see how much simulation resource consumption can be reduced. If the prediction accuracy of regression models for predicting absorption values is high for test scenario C-50, we can conclude that a machine learning model trained with 50% simulation records can accurately predict absorption values for the remaining 50% of wavelengths, and that simulation resource requirements can be cut in half. If regression model prediction accuracy for test scenario C-50 is poor but excellent for test scenario C-30, we can conclude that a machine learning model trained with 70% simulation records can accurately predict absorption values for the remaining 30% of wavelengths, reducing simulation resource requirements by 30%.

KNN-Regressor is a supervised machine learning algorithm used for predicting the continuous-valued target. Working of KNN-Regressor is as follows:

Input:

- Training Dataset 'D'
- Value of 'K'
- Record 'I' for Prediction

Procedure:

- Step 1: Calculate difference between Record 'I' and every record present in dataset 'D'
- Step 2: Select 'K' records from dataset 'D' with the least difference from Record 'I'

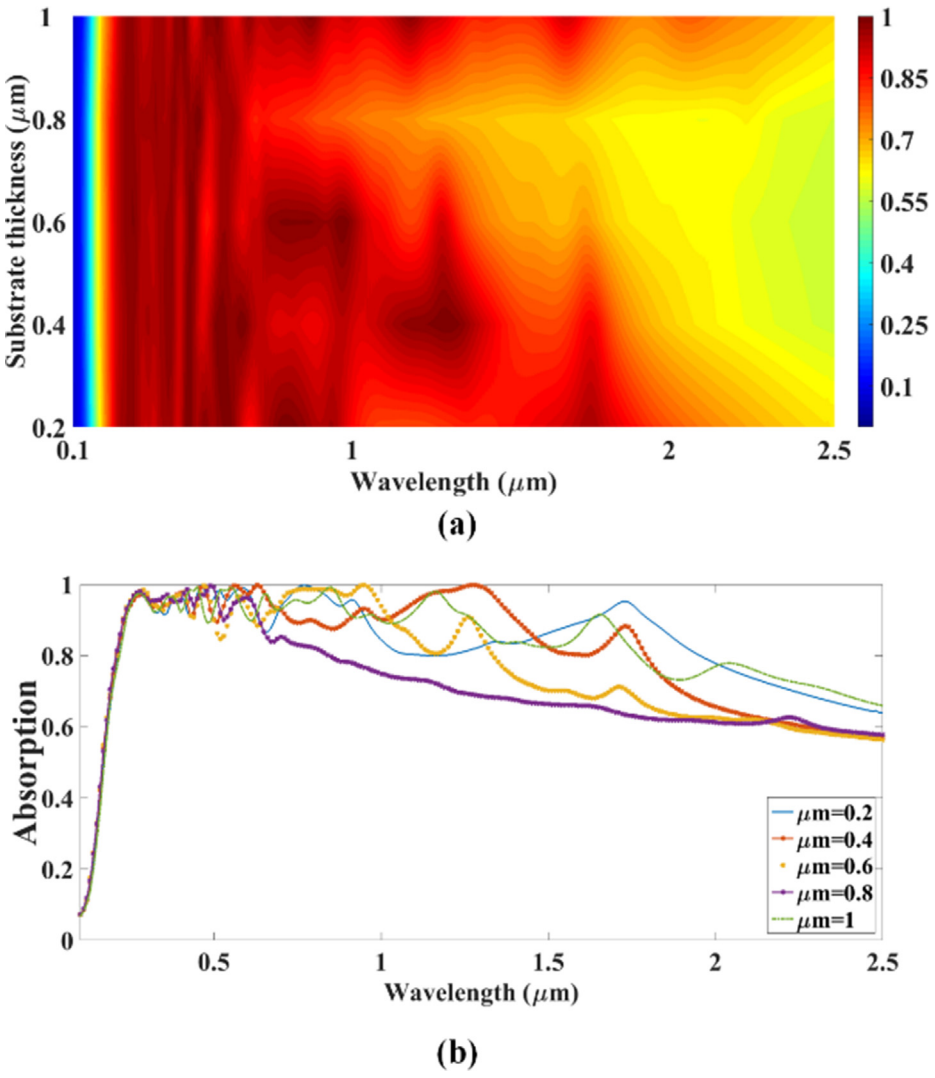

Fig. 4 Substrate thickness variation from 0.2 μm to 1 μm and its effect on absorption (a) 2D plot for spectrum response for different substrate thicknesses. (b) Line plot for different substrate thickness. The average absorption is highest at 0.6 μm.

- Step 3: SUM = Add target labels of 'K' number of closest records
- Step 4: Predicted Target = SUM/K

Euclidian distance is the most commonly used metric to measure the difference between Record 'I' and records present in dataset 'D'. Eq. (5) is used to compute the euclidian distance.

$$difference(I, X) = \sqrt{\sum_{j=1}^{n} (I_j - X_j)^2} \tag{5}$$

Here, n is a number of attributes in the training dataset. R^2 Score is used as a metric to evaluate the performance of KNN-Regressor. It is computed using Eq. (6).

$$R^2 = 1 - \frac{SS_{red}}{SS_{tot}} \tag{6}$$

$$SS_{tot} = \sum_{i=1}^{M} (ActualTarget_i - AverageTargetValue)^2 \tag{7}$$

$$SS_{res} = \sum_{1}^{M} (PredictedTargetValue_i - ActualTargetValue_i)^2 \tag{8}$$

Here, SS_{tot} is total sum of the errors, M is number of records and SS_{res} is sum of squares of the residual errors. Adjusted R^2 score gives more precise view of regression model's prediction accuracy by taking into account number of independent variables. It is calculated using equation (9).

$$Adjusted\ R^2 = 1 - \frac{(1 - R^2)(N - 1)}{(N - p - 1)} \tag{9}$$

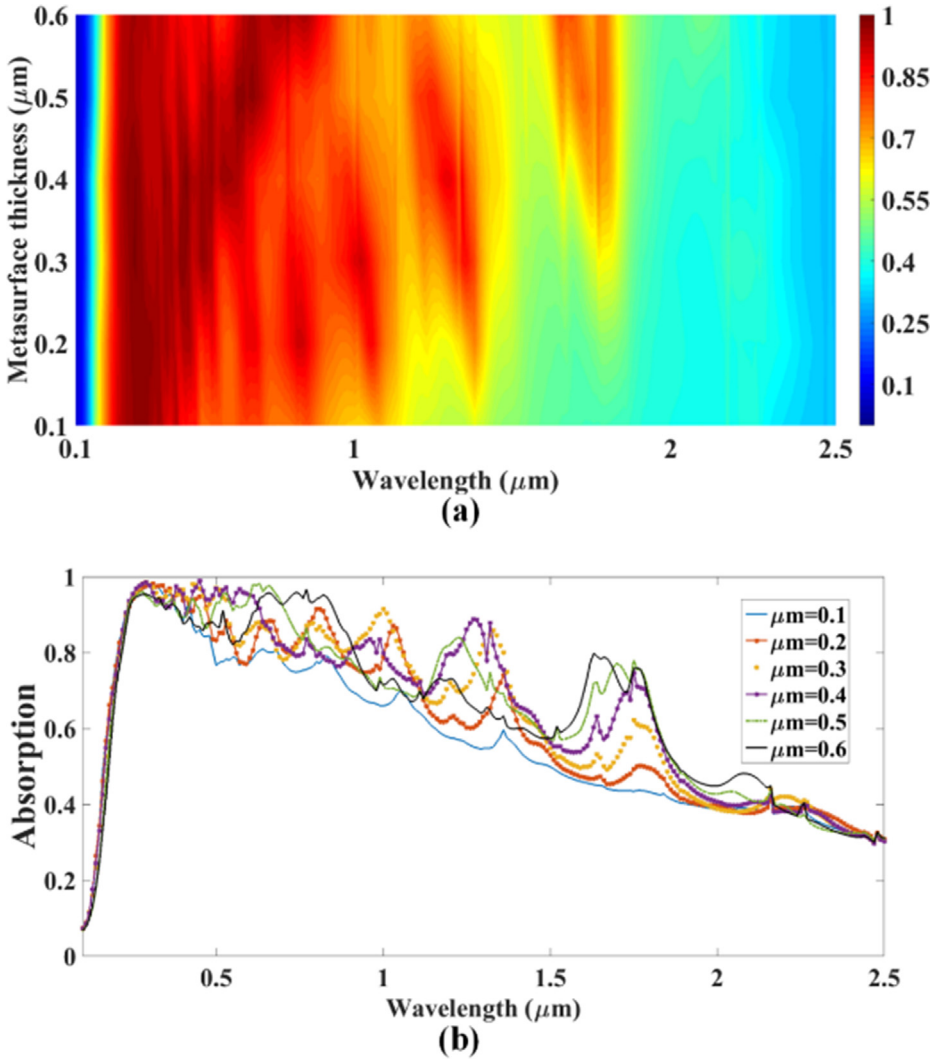

Fig. 5 Metasurface thickness variation from 0.1 μm to 0.6 μm and its effect on absorption (a) 2D plot for spectrum response for different metasurface thickness. (b) Line plot for different metasurface thickness. The average absorption is highest at 0.4 μm.

Here, N is number of samples, R^2 is R^2 score and p is number of independent variables. The adjusted R^2 score of all experimental results is rounded to 3 decimal places. Adjusted R^2 score value close to 1.0 indicates high accuracy of prediction and very low prediction error.

Heatmap depicting adjusted R^2 score attained by KNN-Regressor models trained for assorted combination of 'K' and substrate thickness values under test scenario C-30, C-50 is shown in Fig. 9(a) and (b) respectively. When the 'K' value is 2, an adjusted R^2 Score near to 1.0 is achieved during experimentation for test scenarios C-50 and C-30 for all substrate thickness values. This indicates that simulation resource requirements for assorted substrate thickness values can be decreased by 50 percent.

Heatmap depicting adjusted R^2 score attained by KNN-Regressor models trained for assorted combination of 'K' and ground plane values under test scenario C-30, C-50 is shown in Fig. 10(a) and (b) respectively. When the 'K' value is 2, an adjusted R^2 Score near to 1.0 is achieved during experimentation for test scenarios C-50 and C-30 for all ground plane values. This indicates that simulation resource requirements for assorted ground plane values can be decreased by 50 percent.

Heatmap depicting adjusted R^2 score attained by KNN-Regressor models trained for assorted combination of 'K' and metasurface thickness values under test scenario C-30, C-50 is shown in Fig. 11(a) and (b) respectively. When the 'K' value is 2, an adjusted R^2 Score near to 1.0 is achieved during experimentation for test scenarios C-50 and C-30 for all metasurface thickness values. This indicates that simulation resource requirements for assorted metasurface thickness values can be decreased by 50 percent.

Heatmap showing attained adjusted R^2 Score of polynomial regression models for assorted combinations of different 'K' values with substrate thickness, ground plane, metasurface thickness during 10-fold cross-validation is depicted in supple-

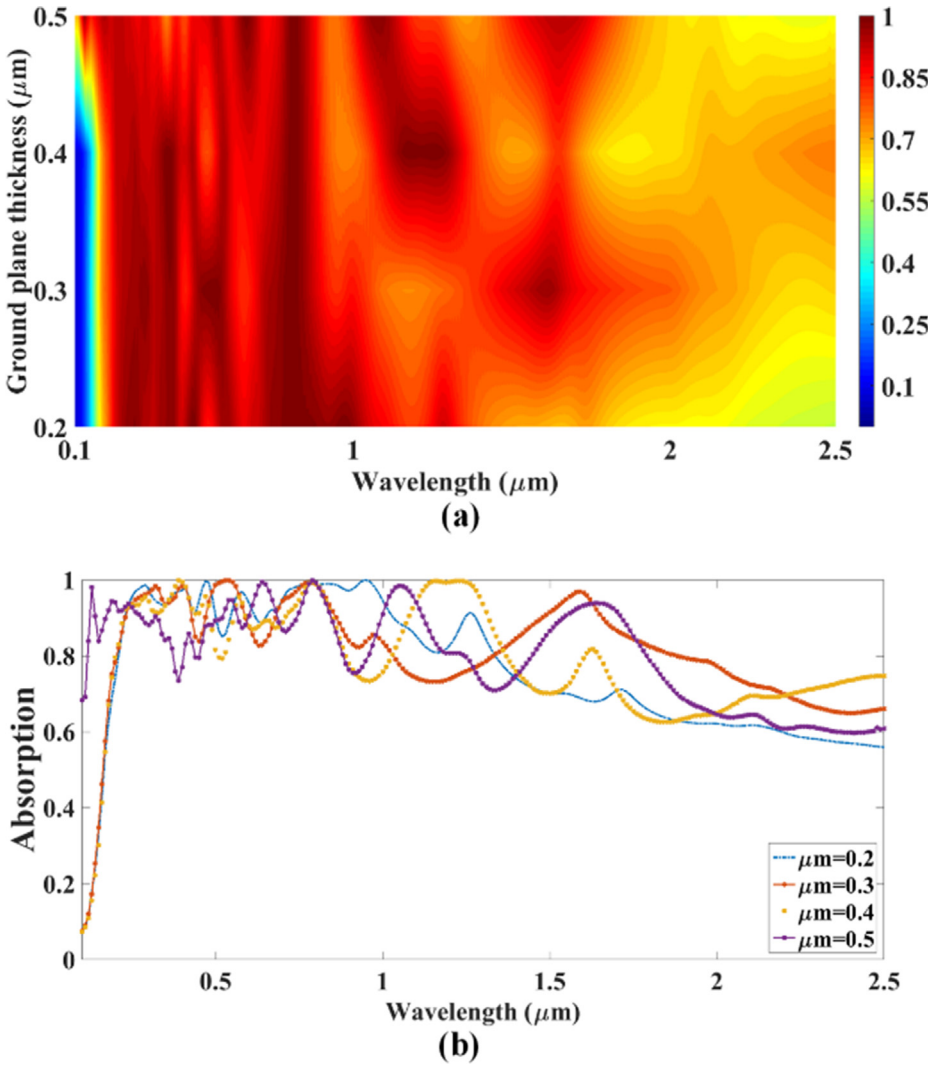

Fig. 6 Ground plane thickness variation from 0.2 μm to 0.5 μm and its effect on absorption (a) 2D plot for spectrum response for different ground plane thickness. (b) Line plot for different ground plane thickness. The response has a minor variation for change in ground plane thickness.

mentary Figs. S1–S3. Adjusted R^2 score values attained during 10-fold cross-validation and test scenarios C-30, C-50 is very close, so it can be concluded that models trained for test scenarios C-30 and C-50 are not overfitted.

Scatter plots of predicted absorption values by KNN-Regressor models during test scenario scenario C-30 vs actual (simulated) absorption values for assorted combinations of different 'K' values with different values of substrate thickness, ground plane, metasurface thickness are shown in Figs. 12–14 respectively. These plots further support the prediction precision of KNN-Regressor models for lower values of K.

Scatter plots of predicted absorption values by KNN-Regressor models during test scenario C-50 vs actual (simulated) absorption values for assorted combinations of different 'K' values with different values of substrate thickness, ground plane, metasurface thickness are shown in supplementary Figs. S4–S6 respectively.

The proposed manuscript presents a novel approach of utilizing phase change material for substrate layer and corresponding results and comparison with previously published work clearly states that the presented work showcases more efficient absorption response. Furthermore, we have applied machine learning based regression model is used to predict

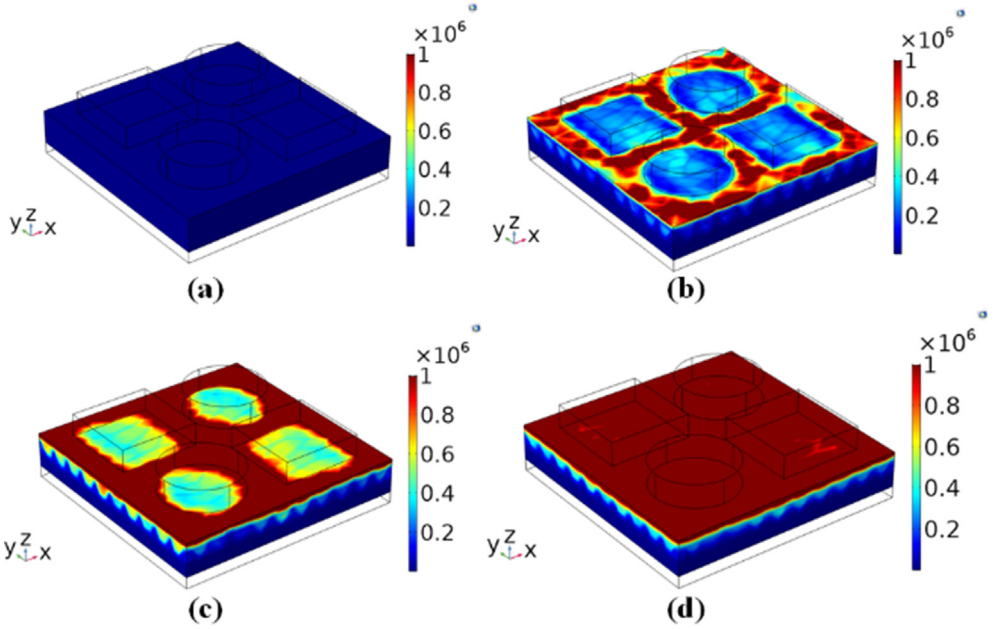

Fig. 7 Electric field response of the metasurface solar absorber design. (a) 0.1 μm (b) 0.5 μm (c) 1 μm (d) 1.5 μm. The light is absorbed in the substrate layer for solar absorber design.

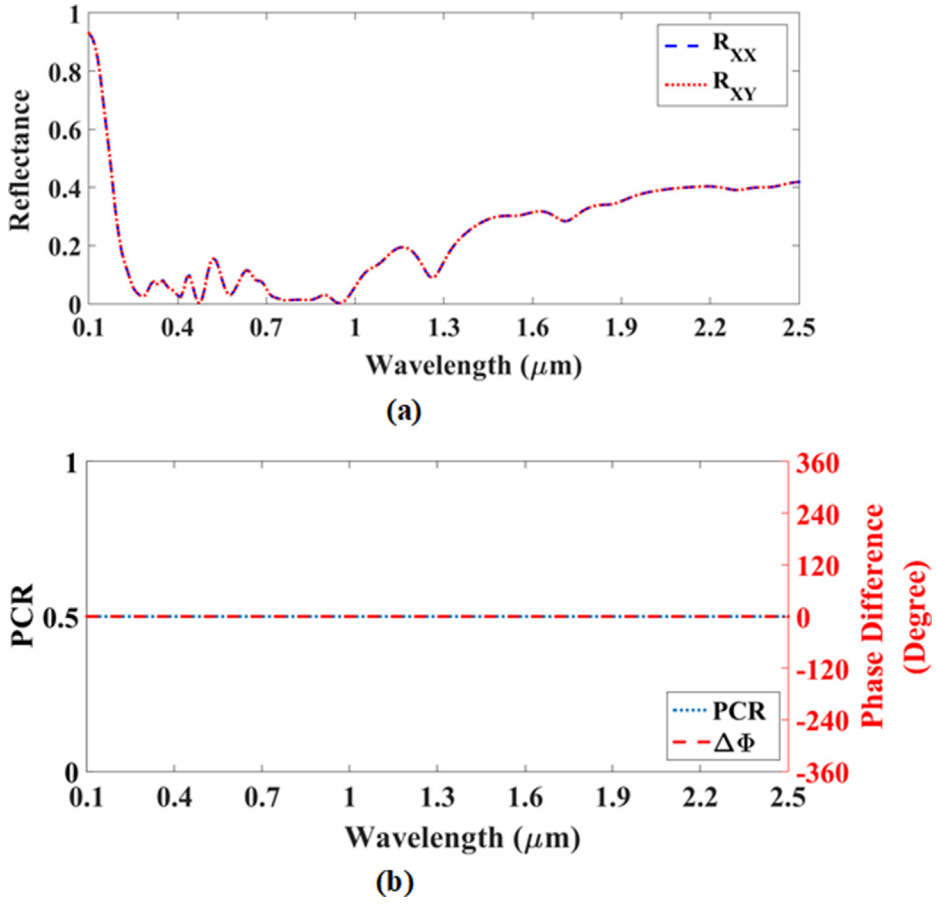

Fig. 8 (a) Reflectance for Co-polarized (Rxx) and Cross-polarized (Rxy) (b) Polarization Conversion Rate and phase difference for GST based metasurface absorber.

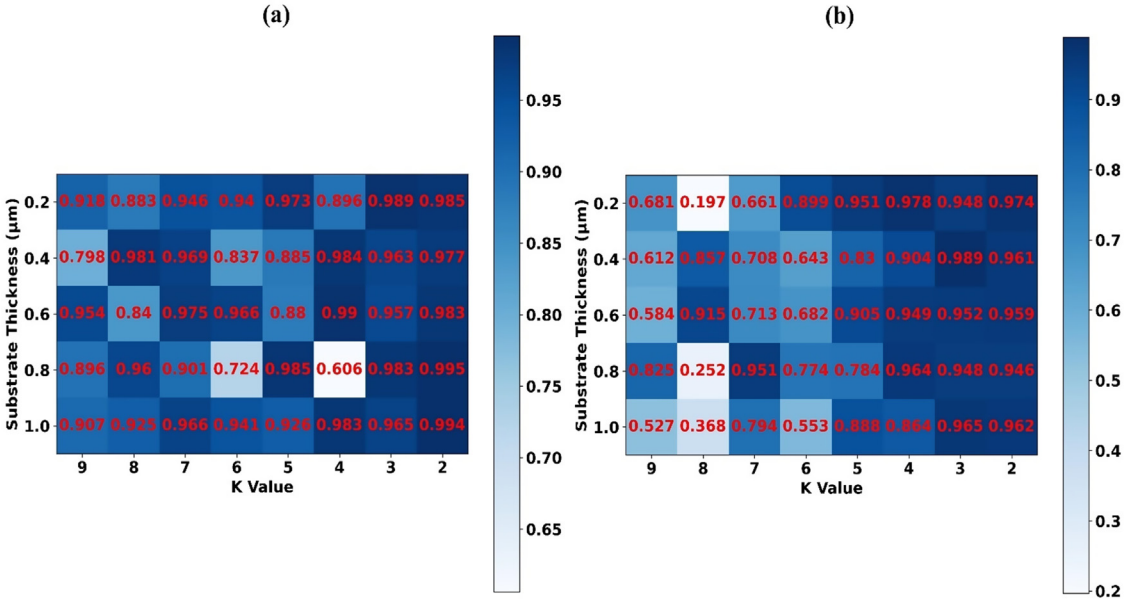

Fig. 9 Prediction efficiency (Adjusted R^2 score) of KNN-Regressor model for different values of Substrate Thickness and 'K' (a) (Test scenario C-30) (b) (Test scenario C-50).

Table 1 Comparison of absorption for two different phases of GST.

Absorption analysis	Ultraviolet Region (0.2–0.39 μm)	Visible Region (0.4–0.7 μm)	Near Infrared Region (0.71–1.5 μm)	All regions (0.2–1.5 μm)
aGST	95.9	93.6	90.6	92
cGST	95.9	92.8	87.7	89.9

Table 2 Comparison of absorption for three different metasurface absorber.

Absorption analysis	Ultraviolet Region (0.2–0.39 μm)	Visible Region (0.4–0.7 μm)	Near Infrared Region (0.71–1.5 μm)	All regions (0.2–1.5 μm)
Square-circle metasurface	95.9	93.6	90.6	92
Circle metasurface	94.2	67.9	72.6	74.1
Square metasurface	93.8	70	67.8	71.4

the values of absorption for intermediate wavelength values. This approach reduces the resources and time required for simulation process.

4. Conclusion

GST-based metasurface solar absorber is presented. The absorber is showing an ultra-broadband response. The absorber is absorbing more than 90% for ultraviolet, visible, and near-infrared regions. The aGST phase gives 92% absorption for these three regions while cGST phase gives 89.9%. Experimental results using machine learning prove that KNN-Regressor can be used as an effective tool for predicting values of absorption of for missing/intermediate wavelengths. Experimental results also show that high prediction accuracy (more than 0.9 adjusted R^2 Score) is achieved using lower values of 'K'. The proposed design absorption results are also compared with previously published absorber designs for all three regions. The proposed design showing improved performance over those designs. The polarization variation results show that the design is polarization insensitive. The design geometrical parameters like substrate thickness, metasurface thickness, and ground plane thickness are optimized by observing absorption for their different values. The optimized values of substrate thickness, metasurface thickness, and ground plane

Table 3 Comparison of GST-based metasurface absorber design with previously published absorber designs.

Design	Absorption Wavelength range (μm)	Average absorption (%)	Polarization Insensitive
Design from Ref. [41]	0.2–0.7	90	Yes
Design from Ref. [42]	0.4–0.8	80	No
Design from Ref. [43]	0.5–1.5	75	No
Design from Ref. [44]	0.3–1.2	85	Yes
Design from Ref. [45]	0.2–0.77	60	No
Design from Ref. [46]	0.3–2.5	85	No
Design from Ref. [47]	0.3–1.5	90	No
Design from Ref. [48]	0.2–0.8	92	–
Design from Ref. [49]	0.36–1.6	90	No
Design from Ref. [50]	0.45–0.8	80	–
Design from Ref. [51]	0.81–1.07	91.8	Yes
Design from Ref. [52]	0.4–0.8	71.1	Yes
Design from Ref. [53]	0.4–1.4	90	–
Design from Ref. [54]	0.4–1.4	90	–
Proposed absorber design (aGST)	0.2–1.5	92	Yes

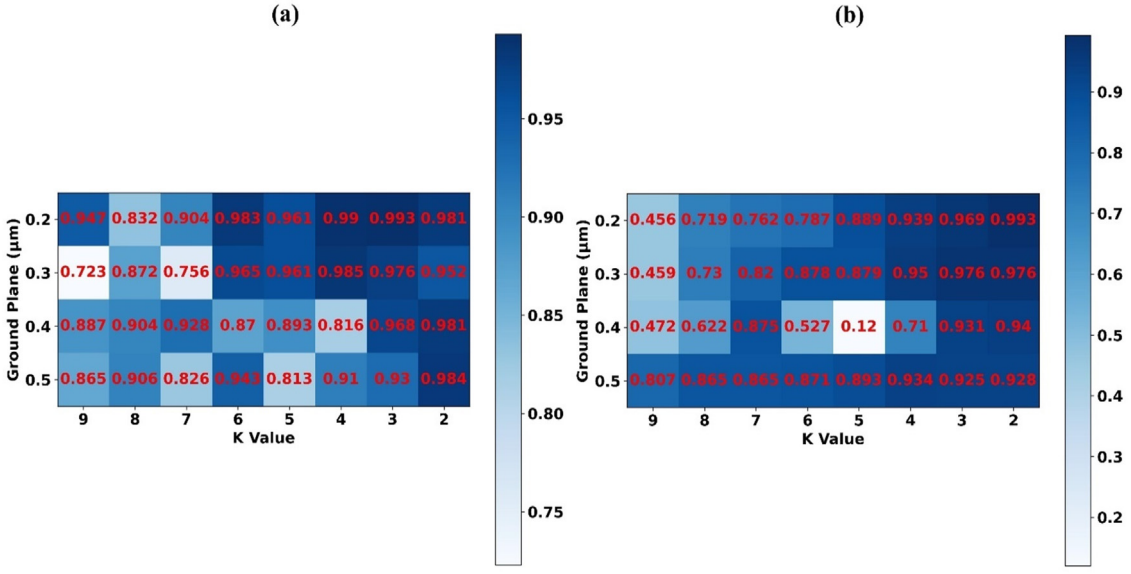

Fig. 10 Prediction efficiency (Adjusted R^2 score) of KNN-Regressor model for different values of Ground Plane and 'K' (a) (Test scenario C-30) (b) (Test scenario C-50).

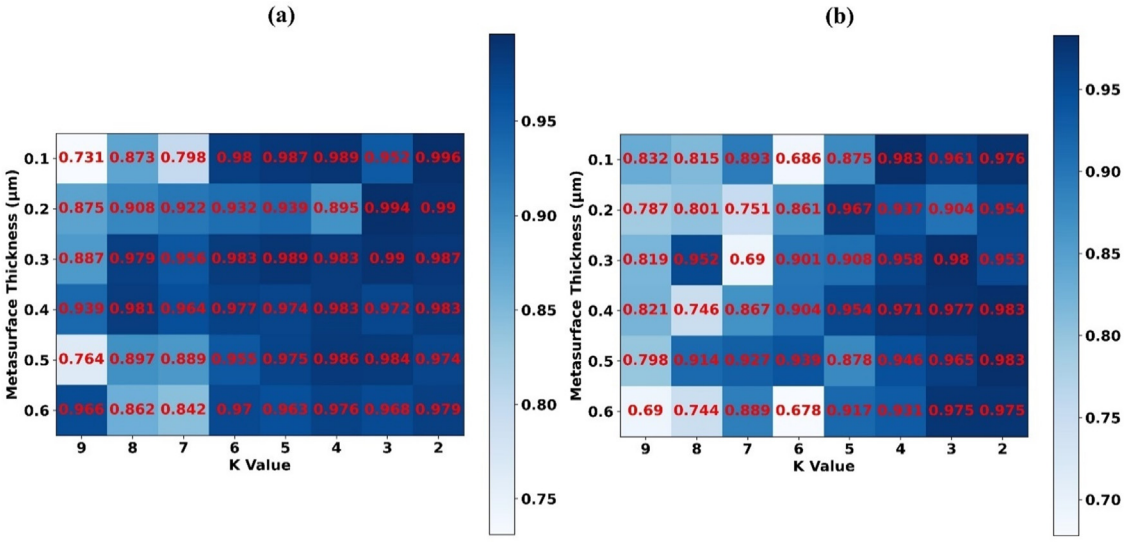

Fig. 11 Prediction efficiency (Adjusted R^2 score) of KNN-Regressor model for different values of Metasurface Thickness and 'K' (a) (Test scenario C-30) (b) (Test scenario C-50).

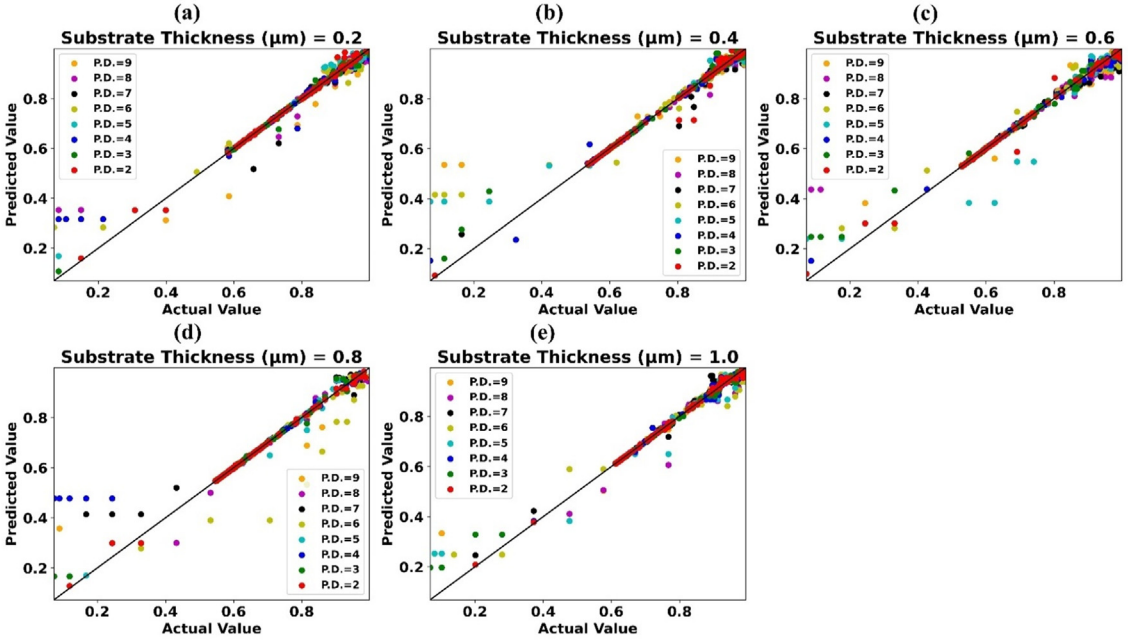

Fig. 12 Predicted absorption values by KNN-Regressor vs actual absorption values for test scenario C-30 and (a) Substrate Thickness = 0.2 μm (b) Substrate Thickness = 0.4 μm (c) Substrate Thickness = 0.6 μm (d) Substrate Thickness = 0.8 μm (e) Substrate Thickness = 1.0 μm.

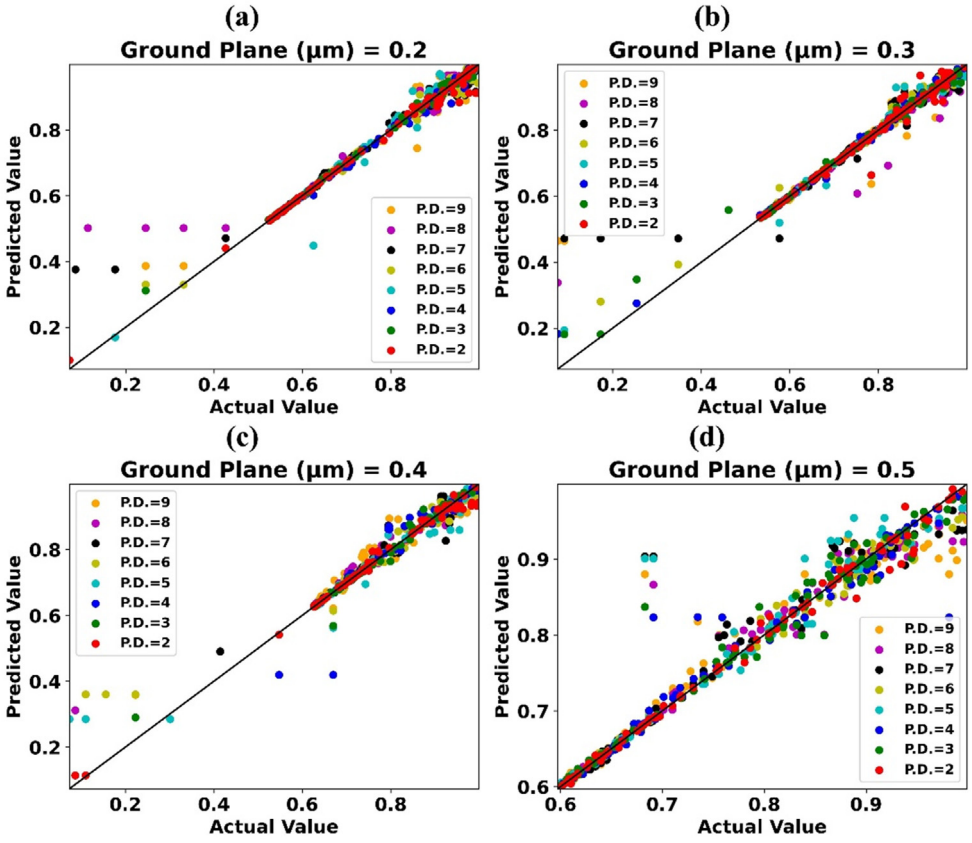

Fig. 13 Predicted absorption values by KNN-Regressor vs actual absorption values for test scenario C-30 and (a) Ground Plane = 0.2 μm (b) Ground Plane = 0.3 μm (c) Ground Plane = 0.4 μm (d) Ground Plane = 0.5 μm.

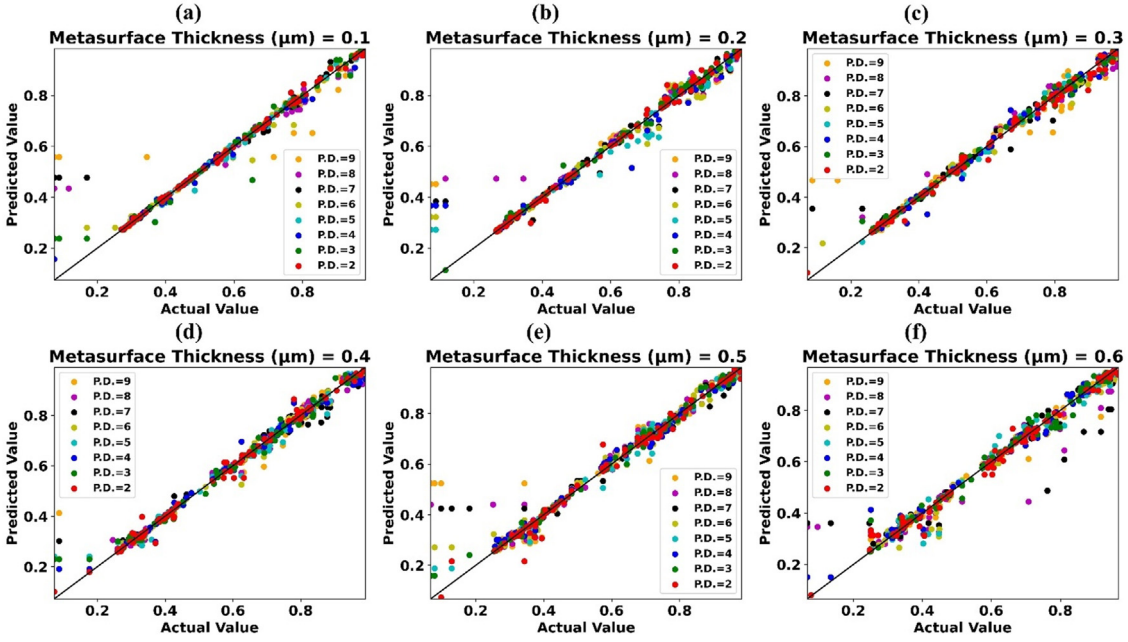

Fig. 14 Predicted absorption values by KNN-Regressor vs actual absorption values for test scenario C-30 and (a) Metasurface Thickness = 0.1 μm (b) Metasurface Thickness = 0.2 μm (c) Metasurface Thickness = 0.3 μm (d) Metasurface Thickness = 0.4 μm (e) Metasurface Thickness = 0.5 μm (f) Metasurface Thickness = 0.6 μm.

thickness are 0.6 μm, 0.4 μm, and 0.2 μm respectively. The GST-based ultra-broadband metasurface solar absorber can become a building block for future solar thermal energy devices. Furthermore, the machine learning approach can also reduce the resources and time required for simulation process.

5. Data availability

The data will be made available at a reasonable request to the corresponding author.

Declaration of Competing Interest

The authors declare that they have no known competing financial interests or personal relationships that could have appeared to influence the work reported in this paper.

Acknowledgement

The authors would like to thank the Deanship of Scientific Research at Umm Al-Qura University for supporting this work by Grant Code: (22UQU4170008DSR03).

Funding

The fund number is 22UQU4170008DSR03.

Appendix A. Supplementary material

Supplementary data to this article can be found online at https://doi.org/10.1016/j.aej.2022.03.080.

References

[1] D. Sciti, L. Silvestroni, L. Mercatelli, J.L. Sans, E. Sani, Suitability of ultra-refractory diboride ceramics as absorbers for solar energy applications, Sol. Energy Mater. Sol. Cells 109 (2013) 8–16, https://doi.org/10.1016/j.solmat.2012.10.004.

[2] Q. Ye, M. Chen, W. Cai, Numerically investigating a wide-angle polarization-independent ultra-broadband solar selective absorber for high-efficiency solar thermal energy conversion, Sol. Energy 184 (2019) 489–496, https://doi.org/10.1016/j.solener.2019.04.037.

[3] N. Mufti, T. Amrillah, A. Taufiq, Sunaryono, Aripriharta, M. Diantoro, Zulhadjri, H. Nur, Review of CIGS-based solar cells manufacturing by structural engineering, Sol. Energy 207 (2020) 1146–1157.

[4] C. Liang, Y. Zhang, Z. Yi, X. Chen, Z. Zhou, H. Yang, Y. Yi, Y. Tang, W. Yao, Y. Yi, A broadband and polarization-independent metamaterial perfect absorber with monolayer Cr and Ti elliptical disks array, Results Phys. 15 (2019) 102635.

[5] S. Ghosh, S. Bhattacharyya, D. Chaurasiya, K.V. Srivastava, An ultrawideband ultrathin metamaterial absorber based on circular split rings, IEEE Antennas Wirel. Propag. Lett. 14 (2015) 1172–1175.

[6] Z. Liu, H. Zhong, H. Zhang, Z. Huang, G. Liu, X. Liu, G. Fu, C. Tang, Silicon multi-resonant metasurface for full-spectrum perfect solar energy absorption, Sol. Energy 199 (2020) 360–365.

[7] J.i. Luo, Y.-S. Lin, High-efficiency of infrared absorption by using composited metamaterial nanotubes, Appl. Phys. Lett. 114 (5) (2019) 051601.

[8] C. Cen, Z. Yi, G. Zhang, Y. Zhang, C. Liang, X. Chen, Y. Tang, X. Ye, Y. Yi, J. Wang, J. Hua, Theoretical design of a triple-band perfect metamaterial absorber in the THz frequency range, Results Phys. 14 (2019) 102463.

[9] J.Y. Chang, H. Wang, L. Wang, Tungsten Nanowire Metamaterials as Selective Solar Thermal Absorbers by Excitation of Magnetic Polaritons, J. Heat Transfer (2017), https://doi.org/10.1115/1.4034845.

[10] C. Wan, Y. Ho, S. Nunez-Sanchez, L. Chen, M. Lopez-Garcia, J. Pugh, B. Zhu, P. Selvaraj, T. Mallick, S. Senthilarasu, M.J. Cryan, A selective metasurface absorber with an amorphous carbon interlayer for solar thermal applications, Nano Energy 26 (2016) 392–397.

[11] J. Si, X. Yu, J. Zhang, W. Yang, S. Liu, X. Deng, Broadened band near-perfect absorber based on amorphous silicon metasurface, Opt. Express 28 (12) (2020) 17900.

[12] J. Liu, W. Chen, W.-Z. Ma, G.-X. Yu, J.-C. Zheng, Y.-S. Chen, C.-F. Yang, Ultra-Broadband Infrared Absorbers Using Iron Thin Layers, IEEE Access 8 (2020) 43407–43412.

[13] S.K. Patel, S. Charola, C. Jani, M. Ladumor, J. Parmar, T. Guo, Graphene-based highly efficient and broadband solar absorber, Opt. Mater. 96 (2019) 109330.

[14] S.K. Patel, J. Parmar, H. Trivedi, R. Zakaria, T.K. Nguyen, V. Dhasarathan, Highly Sensitive Graphene-Based Refractive Index Biosensor Using Gold Metasurface Array, IEEE Photonics Technol. Lett. 32 (12) (2020) 681–684.

[15] A. Li, S. Singh, D. Sievenpiper, Metasurfaces and their applications, Nanophotonics 7 (6) (2018) 989–1011, https://doi.org/10.1515/nanoph-2017-0120.

[16] Y. Chen, Y.-Y. Yue, S.-R. Wang, N. Zhang, J. Feng, H.-B. Sun, Thermally-induced wrinkles on PH1000/graphene composite electrode for enhanced efficiency of organic solar cells, Sol. Energy Mater. Sol. Cells 201 (2019) 110075.

[17] S. Patel, J. Parmar, D. Katrodiya, T.K. Nguyen, E. Holdengreber, Vigneswaran Dhasarathan, Broadband Metamaterial-based Near-infrared Absorber using Array of Uniformly Placed Gold Resonators, J. Opt. Soc. Am. B 37 (7) (2020) 2163–2170, https://doi.org/10.1364/josab.389283.

[18] S.K. Patel, J. Parmar, R.B. Zakaria, S. A., T.K. Nguyen, V. Dhasarathan, Sensitivity Analysis of Metasurface Array-Based Refractive Index Biosensors, IEEE Sens. J. 21 (2) (2021) 1470–1477.

[19] H. Shen, C. Liu, F. Liu, Y. Jin, B. Guo, Z. Wei, F. Wang, C. Tan, X. Huang, H. Meng, Multi-band plasmonic absorber based on hybrid metal-graphene metasurface for refractive index sensing application, Results Phys. 23 (2021) 104020.

[20] X. Zhao, Y. Wang, J. Schalch, G. Duan, K. Cremin, J. Zhang, C. Chen, R.D. Averitt, X. Zhang, Optically Modulated Ultra-Broadband All-Silicon Metamaterial Terahertz Absorbers, ACS Photonics 6 (4) (2019) 830–837.

[21] Z. Liu, G. Liu, Z. Huang, X. Liu, G. Fu, Ultra-broadband perfect solar absorber by an ultra-thin refractory titanium nitride meta-surface, Sol. Energy Mater. Sol. Cells 179 (2018) 346–352, https://doi.org/10.1016/j.solmat.2017.12.033.

[22] B. Qi, Y. Zhao, T. Niu, Z. Mei, Ultra-broadband metamaterial absorber based on all-metal nanostructures, J. Phys. D. Appl. Phys. 52 (42) (2019), https://doi.org/10.1088/1361-6463/AB31FF 425304.

[23] W. Guo, Y. Liu, T. Han, Ultra-broadband infrared metasurface absorber, Opt. Express 24 (18) (2016) 20586, https://doi.org/10.1364/oe.24.020586.

[24] Y. Shi, Y.C. Li, T. Hao, L. Li, C.-H. Liang, A design of ultra-broadband metamaterial absorber, Waves in Random and Complex Media 27 (2) (2017) 381–391.

[25] R. Jadeja, S. Charola, S.K. Patel, J. Parmar, M. Ladumor, T.K. Nguyen, V. Dhasarathan, Numerical investigation of graphene-based efficient and broadband metasurface for terahertz solar absorber, J. Mater. Sci. 55 (8) (2020) 3462–3469.

[26] Y.K. Zhong, S.M. Fu, W. Huang, D. Rung, J.-W. Huang, P. Parashar, A. Lin, Polarization-selective ultra-broadband super absorber, Opt. Express 25 (4) (2017) A124.
[27] S.K. Patel, J. Surve, J. Parmar, T.K. Nguyen, Review on Graphene-based Absorbers for Infrared to Ultraviolet Frequencies, J. Adv. Eng. Comput. 5 (4) (2021) 214.
[28] H. Liu, M. Xie, Q. Ai, Z. Yu, Ultra-broadband selective absorber for near-perfect harvesting of solar energy, J. Quant. Spectrosc. Radiat. Transf. 266 (2021) 107575.
[29] J. Jiang, Y. Xu, Y. Li, L. Ren, F. Chen, S. Cheng, W. yang, C. Ma, Z. Wang, X. Zhou, Ultra-broadband, near-perfect and thin-film scale solar absorber based on semiconductor-metal nanocone, Optik (Stuttg) 246 (2021) 167855.
[30] H. Feng, X. Li, M. Wang, F. Xia, K. Zhang, W. Kong, L. Dong, M. Yun, Ultrabroadband metamaterial absorbers from ultraviolet to near-infrared based on multiple resonances for harvesting solar energy, Opt. Express 29 (4) (2021) 6000.
[31] S. Raoux, Phase change materials, Annu. Rev. Mater. Res. 39 (1) (2009) 25–48.
[32] Z. Guo, X. Yang, F. Shen, Q. Zhou, J. Gao, K. Guo, Active-Tuning and Polarization-Independent Absorber and Sensor in the Infrared Region Based on the Phase Change Material of Ge2Sb2Te5 (GST), Sci. Rep. 8 (1) (2018), https://doi.org/10.1038/s41598-018-30550-2.
[33] S. Abdollahramezani, O. Hemmatyar, H. Taghinejad, A. Krasnok, Y. Kiarashinejad, M. Zandehshahvar, A. Alù, A. Adibi, Tunable nanophotonics enabled by chalcogenide phase-change materials, Nanophotonics 9 (5) (2020) 1189–1241.
[34] S.K. Patel, C. Argyropoulos, A. Christos, M. Alessio, Plasmonic nanoantennas: Enhancing light-matter interactions at the nanoscale, EPJ Appl. Metamater. 2 (2015) 4.
[35] X. Zhang, Z. Du, Y. Zhu, C. Li, X. Hu, T. Yang, B.-B. Yu, R. Gu, Y. Ding, Z. He, A novel volumetric absorber integrated with low-cost D-Mannitol and acetylene-black nanoparticles for solar-thermal-electricity generation, Sol. Energy Mater. Sol. Cells 207 (2020) 110366.
[36] Y.G. Chen, T.S. Kao, B. Ng, X. Li, X.G. Luo, B. Luk'yanchuk, S.A. Maier, M.H. Hong, Hybrid phase-change plasmonic crystals for active tuning of lattice resonances, Opt. Express 21 (11) (2013) 13691.
[37] M. Wei, Z. Song, Y. Deng, Y. Liu, Q. Chen, Large-angle mid-infrared absorption switch enabled by polarization-independent GST metasurfaces, Mater. Lett. 236 (2019) 350–353.
[38] T. Guo, C. Argyropoulos, Broadband polarizers based on graphene metasurfaces, Opt. Lett. 41 (23) (2016) 5592.
[39] S.K. Patel, S. Charola, R. Suresh Kumar, J. Parmar, Broadband polarization-insensitive Jerusalem-shaped metasurface absorber based on phase-change material for the visible region, Phys. B Condens. Matter 624 (2022) 413440.
[40] S.K. Patel, J. Parmar, V. Katkar, Metasurface-based solar absorber with absorption prediction using machine learning, Opt. Mater. 124 (2022) 112049.
[41] C. Li, H. Fan, Q. Dai, Z. Wei, S. Lan, H. Liu, Multipole resonance in arrays of diamond dielectric: A metamaterial perfect absorber in the visible regime, Nanomaterials 9 (9) (2019) 1222.
[42] Z. Liu, X. Liu, S. Huang, P. Pan, J. Chen, G. Liu, G. Gu, Automatically acquired broadband plasmonic-metamaterial black absorber during the metallic film-formation, ACS Appl. Mater. Interfaces 7 (8) (2015) 4962–4968.
[43] N. Muhammad, X. Tang, F.u. Tao, L. Qiang, O. Zhengbiao, Broadband polarization-insensitive absorption by metasurface with metallic pieces for energy harvesting application, Mater. Sci. Eng. B Solid-State Mater. Adv. Technol. 249 (2019) 114419.
[44] H. Zhang, M. Luo, Y. Zhou, Y. Ji, L. Chen, Ultra-broadband, polarization-independent, wide-angle near-perfect absorber incorporating a one-dimensional meta-surface with refractory materials from UV to the near-infrared region, Opt. Mater. Express 10 (2) (2020) 484.
[45] M.J. Hossain, M.R.I. Faruque, M.R. Ahmed, M.J. Alam, M.T. Islam, Polarization-insensitive infrared-visible perfect metamaterial absorber and permittivity sensor, Results Phys. 14 (2019) 102429.
[46] H. Lin, B.C.P. Sturmberg, K.-T. Lin, Y. Yang, X. Zheng, T.K. Chong, C.M. de Sterke, B. Jia, A 90-nm-thick graphene metamaterial for strong and extremely broadband absorption of unpolarized light, Nat. Photonics 13 (4) (2019) 270–276.
[47] M. Chen, Y. He, Plasmonic nanostructures for broadband solar absorption based on the intrinsic absorption of metals, Sol. Energy Mater. Sol. Cells 188 (2018) 156–163.
[48] J. Surve, J. Parmar, S.K. Patel, R. Jadeja, Comparative analysis of metasurface array-based solar absorber for visible region, Opt. Quantum Electron. 53 (12) (2021) 696, https://doi.org/10.1007/s11082-021-03355-3.
[49] P. Yu, X. Chen, Z. Yi, Y. Tang, H. Yang, Z. Zhou, T. Duan, S. Cheng, J. Zhang, Y. Yi, A numerical research of wideband solar absorber based on refractory metal from visible to near infrared, Opt. Mater. (Amst) 97 (2019) 109400.
[50] B. Liu, C. Tang, J. Chen, N. Xie, H. Tang, X. Zhu, G.-S. Park, Multiband and Broadband Absorption Enhancement of Monolayer Graphene at Optical Frequencies from Multiple Magnetic Dipole Resonances in Metamaterials, Nanoscale Res. Lett. 13 (1) (2018), https://doi.org/10.1186/s11671-018-2569-3.
[51] S.K. Patel, S. Charola, R. Jadeja, T.K. Nguyen, V. Dhasarathan, Wideband graphene-based near-infrared solar absorber using C-shaped rectangular sawtooth metasurface, Phys. E Low-Dimens. Syst. Nanostruct. 126 (2021), https://doi.org/10.1016/j.physe.2020.114493 114493.
[52] T. Sang, J. Gao, X. Yin, H. Qi, L. Wang, H. Jiao, Angle-Insensitive Broadband Absorption Enhancement of Graphene Using a Multi-Grooved Metasurface, Nanoscale Res. Lett. 14 (2019), https://doi.org/10.1186/s11671-019-2937-7.
[53] X. Tian, Z.-Y. Li, Visible-near infrared ultra-broadband polarization-independent metamaterial perfect absorber involving phase-change materials, Photonics Res. 4 (4) (2016) 146, https://doi.org/10.1364/prj.4.000146.
[54] H. Xu, L. Hu, Y. Lu, J. Xu, Y. Chen, Dual-Band Metamaterial Absorbers in the Visible and Near-Infrared Regions, J. Phys. Chem. C 123 (15) (2019) 10028–10033, https://doi.org/10.1021/acs.jpcc.9b00434.